

Automatic Feedback Control in Electron Beam Melting Using Infrared Thermography

Jorge Mireles¹, Cesar Terrazas¹, Francisco Medina¹, Ryan Wicker¹

1. W.M. Keck Center for 3D Innovation, The University of Texas at El Paso, El Paso, TX

Accepted August 16th 2013

Abstract

An infrared (IR) camera has been installed in an Arcam A2 Electron Beam Melting (EBM) system for improved layer-by-layer monitoring and feedback control of the EBM build process. Previous work has demonstrated the temperature variations possible during a build (e.g., part/powder bed temperature elevates as build height increases) that have been shown to produce microstructural changes as well as a range of defects that can be detected (e.g., temperature anomalies and porosity). A stabilization of temperature during a build can lead to more uniform microstructure and mechanical properties throughout the fabricated part. Further, full spatial and temporal control of temperature could lead to controlled microstructural architectures in EBM-fabricated parts. An automatic feedback control system was developed to acquire a temperature matrix of the current layer and used as an input to a ‘ghost operator’ that modifies the necessary parameters (speed function, beam current, melt cycle’s post-heating time) for temperature stabilization to minimize microstructural variations.

Introduction

The Electron Beam Melting (EBM) process has been a promising technology for the rapid manufacturing of end-use metal components. Several materials have been processed using EBM (e.g. Ti-6Al-4V, Inconel 625, and Inconel 718) that are of interest in the aerospace industry for flight-ready part fabrication (Rodriguez *et al.*, 2012, Murr *et al.*, 2011). Although part fabrication using Ti-6Al-4V has resulted in dense parts with mechanical properties comparable to wrought titanium, several anomalies in microstructure still exist, namely differences in microstructure throughout a part that are due to a thermal gradient within the build chamber during fabrication (Murr *et al.*, 2009; Puebla *et al.*, 2012). Such uncontrolled variations are not suitable when mechanically isotropic parts are needed. Furthermore, if a higher level of control is present in EBM, it may be possible to fabricate mechanically isotropic parts or parts with prescribed anisotropy, ensure manufacturing repeatability and reproducibility, and meet an adequate level of quality.

A FLIR SC645 infrared (IR) camera was installed in an Arcam A2 EBM system for the purpose of layer-by-layer monitoring and feedback (Rodriguez *et al.*, 2012). Studies were performed observing parts produced using Ti-6Al-4V and results included the detection of defects such as porosity, non-uniform temperature between parts in a single build, non-uniform temperature within a single part, and over-melt of powder. Using the improved feedback from the IR system, an operator was able to manually modify parameters to achieve a more uniform build temperature (Rodriguez, 2012). The current research focuses on developing an automatic feedback control method in an attempt to achieve a uniform build temperature to attain microstructural uniformity, detect defects, and achieve a layer-by-layer control of parameters to change grain size in Ti-6Al-4V microstructure.

Concept

Microstructural gradients in EBM-fabricated parts have been previously studied. These results show grain size differences from the bottom of a build to the top of a build where the bottom of a build exhibits a finer microstructure than the top of a build (Murr *et al.*, 2009). Differences in grain size have been attributed to changes in mechanical properties such as hardness, ultimate tensile strength, and elongation (Murr *et al.*, 2009, Puebla *et al.*, 2012). Moreover, some microstructural differences still exist after performing a HIP operation (Mireles *et al.*, 2013). The layer-by-layer control achieved using an automatic feedback control loop can either attempt to stabilize process temperature to achieve uniform grain size or attempt to purposely increase/decrease process temperature through parameter modifications in an attempt to achieve a desired grain size or grain size gradient part. The basic concept for grain growth is described by the following grain growth equation (Porter & Easterling, 1981):

$$D_2^2 = D_0^2 + Kt$$

where D_2 is the final grain size, D_0 is the initial grain size, K is a constant relating heating temperature and activation energy for grain growth, and t is time. Although these fundamental equations are formulated to apply to single-phase metals, studies on Ti-6Al-4V by *Gil and Planell, 2000*, showed such kinetics for grain growth apply for this alloy. As a result, as temperature rises, growth rate increases, and further increases with time when subjected to a high temperature (*Gil & Planell, 2000*). Additionally, performing heat treatment operations such as HIPing of EBM fabricated Ti-6Al-4V parts has shown to increase grain size due to the exposure of a high-temperature cycle that allows grain growth (*Al-Bermani et al., 2010*). Thus, grain growth is both time and temperature dependent.

Methods

Image acquisition after the melt of each layer using an IR camera was previously achieved through the installation of a shutter mechanism and the use of National Instruments hardware and virtual instruments from LabVIEW software (Rodriguez, 2013). In the present work, a virtual instrument was developed to perform automatic control from feedback obtained by images from the IR camera and layer information deciphered from calculations made by the virtual instrument's loop iterations. The lack of a direct application programming interface (API) restricted direct communication with the Arcam EBM Control software to interact and change parameters programmatically on-demand. Therefore, applications were developed which triggered mouse click events to interact with the EBM Control interface using Microsoft Visual Basic 2010, consisting of (1) a program that allowed mapping the X and Y coordinates of different elements within the user interface (buttons, menus, lists, etc.) and (2) a routine that read the mapped coordinate values and triggered the mouse clicks. When called by the image acquisition virtual instrument, the simulation of mouse clicks began to change each parameter accordingly. Two computers were used due to the large memory consumption of image processing that may cause EBM system failure. Communication between the two computing systems was achieved through an Ethernet protocol.

The developed application relies on data from a log file that must be initialized by the operator prior to the start of an experiment or build. Missing this step will cause an

exception error when calling the mouse-triggering application potentially crashing execution of the entire monitoring system. An even simpler source of error can result if the computer mouse is manually moved while the application is called. This will give inaccurate coordinate values to the application resulting in unchanged or falsely changed parameters. Furthermore, the application will not have any effect if the computer screen is locked. Finally, the mapping of the coordinates is specific to the monitor of the Arcam A2 machine used. Therefore, recalibration will be necessary if this application is to be used in another EBM system.

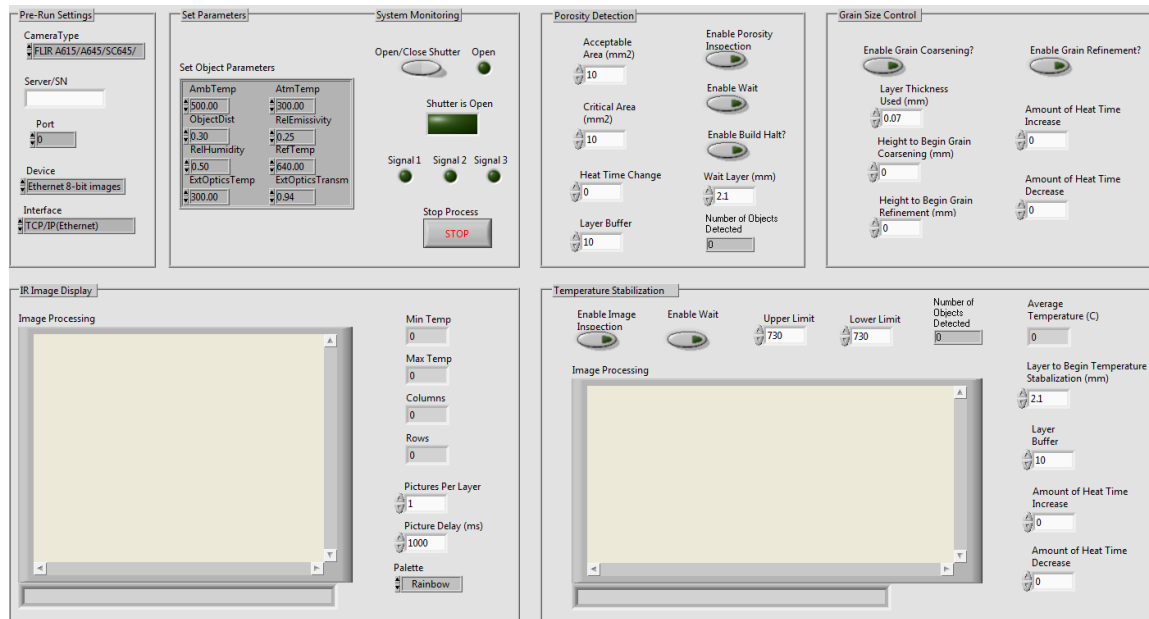


Figure 1 Virtual Instrument for image acquisition and processing

The image acquisition virtual instrument is shown in Figure 1 and requires basic inputs from the operator including number of pictures per layer desired and its corresponding time delay from the instance the melt step has finished (images are taken after a melt step has ended). Included in the virtual instrument were options to run a grain size control algorithm, a temperature stabilization algorithm that performed image processing to detect parts and read average temperature of parts, and a porosity detection algorithm that used previous acquired images of porosity in EBM-fabricated parts as a reference for detection. Five operator inputs were required to run the grain size control algorithm including layer thickness (0.07mm for Ti-6Al-4V), layer to begin parameter changes to achieve coarse grains (units in mm), layer to begin parameter changes to achieve refinement of grains (units in mm), and amount to change parameters (only post-heating time is shown here with units of seconds) for both coarsening and refinement of grains. Six operator inputs were required to run temperature stabilization including upper and lower limits to account for IR measurement error (typically a desired temperature \pm 30-40°C), a layer height to begin stabilization (typically \sim 2mm to account for initial temperature decay), a layer buffer (typically 6-10 to allow for parameters to take effect), and amount of post-heating time increase/decrease for parameter changes when temperature was found to be outside the desired limits.

Using the image acquisition virtual instrument for grain size control, a 16mm diameter by 30mm long cylindrical specimen was fabricated as shown by Figure 2(a). The virtual instrument utilized a counter within its loop structure to compute the current layer and compared it against the user input for desired height for changes to take effect. To obtain a part containing a grain size gradient, a single parameter for the melt cycle post-heating time was increased at 10mm and 20mm from the standard of 25seconds to 45seconds and again from 45seconds to 15seconds, respectively.

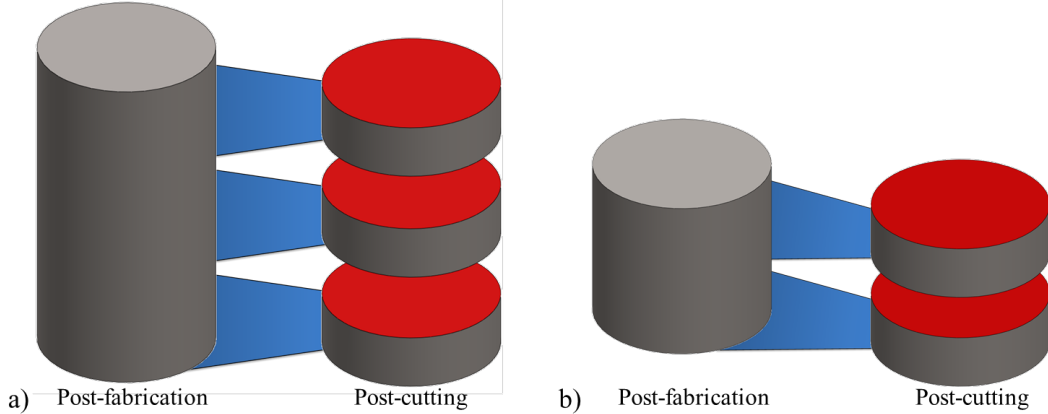


Figure 2 Fabricated specimens and cut sections for a) grain size control and b) temperature stabilization where the red faces are the sections whose microstructure was analyzed

A second cylinder (16mm diameter by 20mm long) was fabricated using a different build to test the temperature stability algorithm and porosity detection algorithm (Figure 2(b)). To perform temperature stability and porosity detection, an image processing step was utilized that performed an image conversion step from the initially grayscale image into a binary image. A part was detected from a pre-defined region of interest and segmentation was achieved by applying an intensity threshold that was defined using previously acquired images of dark intensity level of 195. For temperature stabilization, an average temperature was recorded for the detected part that was used for comparison against the user's temperature range input. The porosity algorithm also used segmentation procedures by applying an intensity threshold to a bright intensity level of 185 that has also been previously defined by images containing porous parts. A numerical amount of porosity was detected and porosity area was measured based on a calibration performed in the algorithm that took pixel size (0.175mm) and computed a total area. The amount of porosity that was measured can be used to compare against a user defined “acceptable range of porosity” in parts (e.g. stop a build if porosity has been detected or continue fabrication if a small amount of porosity is acceptable).

After fabrication, the cylinders were cut using an IsoMet 400 Precision Saw (Buehler, Lake Bluff, IL) into three sections (Figure 2) including a section from the bottom corresponding to a standard post-heating time of 25 seconds for the melt step, a middle section with an elevated post-heating time of 45 seconds, and a top section with a lower post-heating time of 15 seconds. Cylinders fabricated to test the temperature stabilization algorithm were analyzed at the top and bottom sections ~10mm apart as shown by Figure 2. After cutting, the sectioned pieces were mounted with a KoldMount

(CMP Industries, Inc., Albany, NY) specimen mounting resin. Metallography was performed using 80grit, 320grit, 500grit, 800grit, 1000grit, and 1200grit, followed by a finishing step with a polishing cloth using 0.1μ and 0.05μ alumina slurry. An etchant composed of 100ml distilled water (H_2O), 5ml nitric acid (HNO_3), and 2.5ml hydrofluoric acid (HF) was applied for ~15seconds to reveal the microstructure. Optical microscopy was performed on the mounted pieces using a Leica MEF4M optical microscope with a digital imaging system.

Results

Temperature measurements were taken from IR images and recorded versus time as shown in Figure 3(a) where the sections are labeled corresponding to the standard build's post-heating time parameter, grain coarsening section obtained during the increased post-heating time parameter, and grain refinement section corresponding to the decreased post-heating time parameter. IR images for each section were taken and are shown in Figure 3(b) displaying differences in IR temperature obtained by changing heat time parameters. Each measurement is an average of a cylinder's melt area and the variations shown by Figure 3(a) can be due to porosity that may be inside the measurement area. Figure 4 shows the results for the microstructural analysis performed showing standard grain structure when a) standard post-heating time parameters were utilized, coarsened grains when b) increased post-heating time parameters were utilized, and refined grains at c) where lowered post-heating time parameters were utilized. All optical images in this study correspond to acicular α -plate Widmanstätten-like microstructure (Murr *et al.*, 2009). Measurements pertaining to the α grain width for the standard post-heating time parameters were $\sim 0.65\mu m$, $\sim 1.31\mu m$ for the elevated post-heating time, and $\sim 0.96\mu m$ for the lowered post-heating time. Although the post-heating time setting of the top section was reduced below that of the standard, a smaller grain size was not achieved due to the thermal gradient that caused α grain growth in vertically fabricated parts (Puebla *et al.*, 2012). A further reduction in grain size may not have been achieved since other factors such as build time or part size may affect grain growth. Volume of heat for a build can vary from build to build and layer-to-layer thus grain growth for varying build heights, overall part size, and/or heating/cooling time may contribute to grain size variations. Nonetheless, it is noteworthy that the final grain size remained below $\sim 1.31\mu m$ and further coarsening was not evident.

Figure 5 shows the functioning temperature stabilization interface displaying part detection and temperature measurements. A conditional statement was used in the algorithm to change parameters when the temperature was detected beyond the specified limits. It continued building normally when the temperature was detected within the specified temperature limits. Figure 6 shows the microstructure achieved after running the algorithm. Measurements pertaining to the α grain width are $0.62\mu m$ for the bottom and $0.98\mu m$ for the top. Under the rationale that a stable build temperature should result in a constant grain size, the parameter modifications performed were not sufficient to stabilize the build temperature as evidenced from a $\sim 0.36\mu m$ difference in grain size from

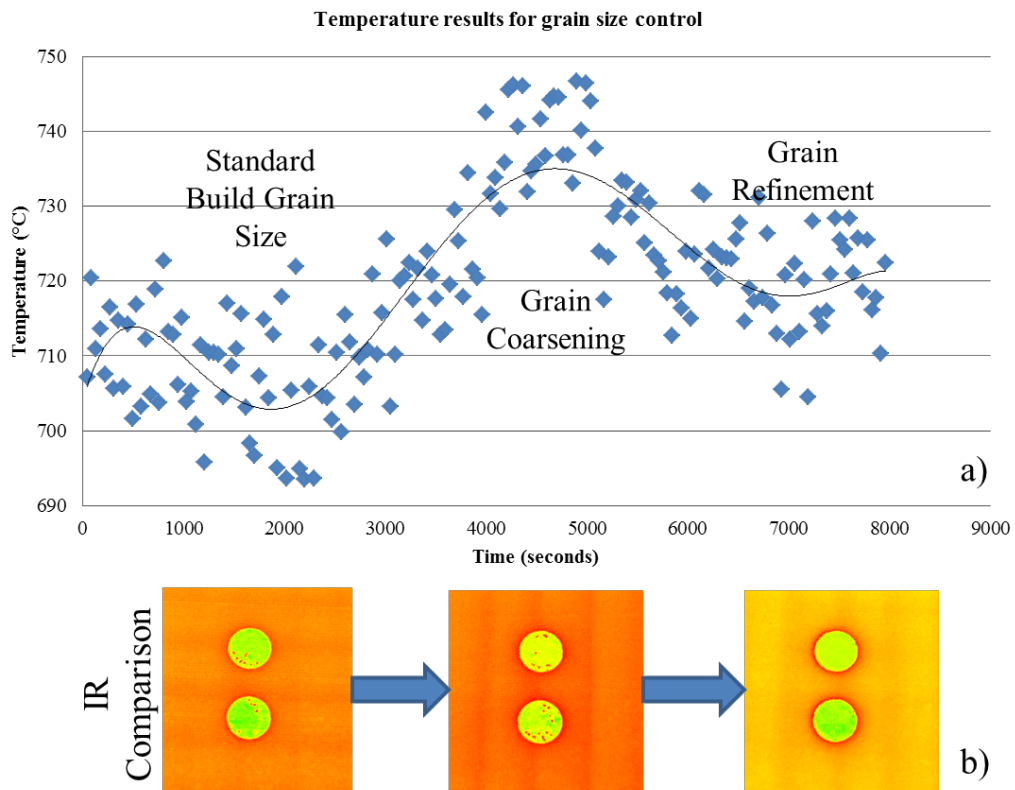


Figure 3 Grain growth experiment showing a) temperature graph from IR images and b) IR image comparison for each standard, coarsened, and refined grain sections where red spots on melt area are porosity that occurred during fabrication

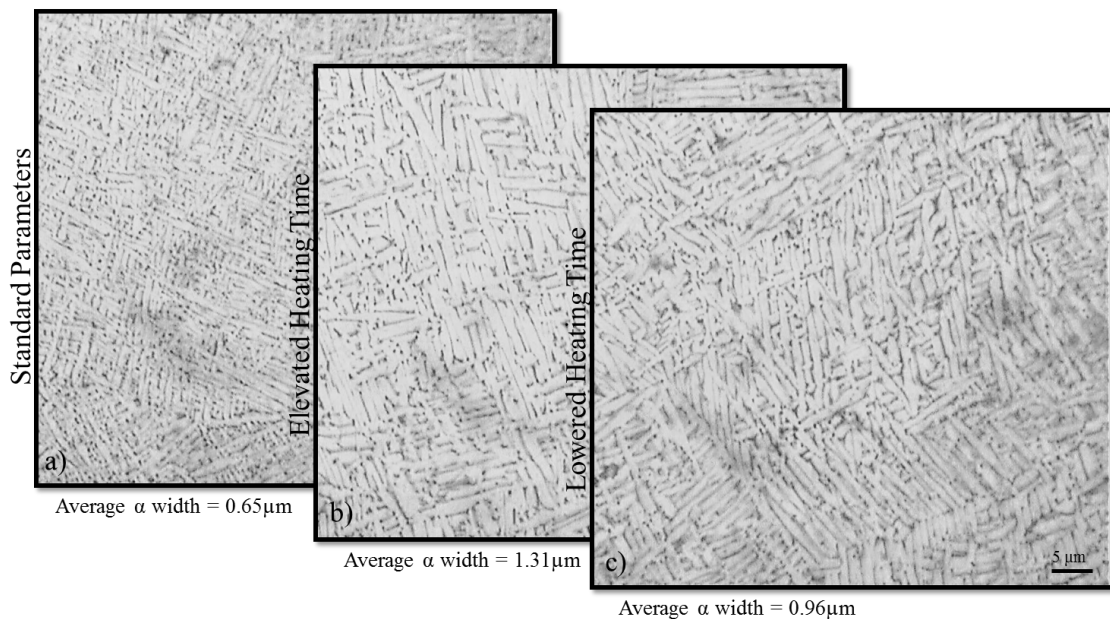


Figure 4 Microstructure images of grain sizes for each section a) standard post-heating time, b) elevated post-heating time parameters, and c) lowered post-heating time parameters

the bottom to the top of the part. Figure 7 shows the temperature measurements taken from the IR images for the temperature stabilization experiment and still shows a slight climb in temperature through fabrication. Several factors may be attributed to the inability to acquire grain uniformity such as uncertainty in the IR temperature measurements that gives variable temperature readings from one layer to the next as well as build temperature variations that may be present in IR images resulting from the build process (Rodriguez, 2013). Furthermore, the changes were only performed by increment/decrement of 2seconds thus it may not be sufficient to produce the desired temperature change. In addition, although the part continued building for both the temperature stabilization and grain growth algorithm, parts exhibited porosity after several parameter changes that may require either a different parameter or a group of parameters to be changed. A method that can help achieve uniform microstructure from the bottom of the build to the top of the build is to achieve a higher level of build chamber temperature control where either temperature is lowered as a build progresses or the build chamber temperature is maintained constant throughout a build.

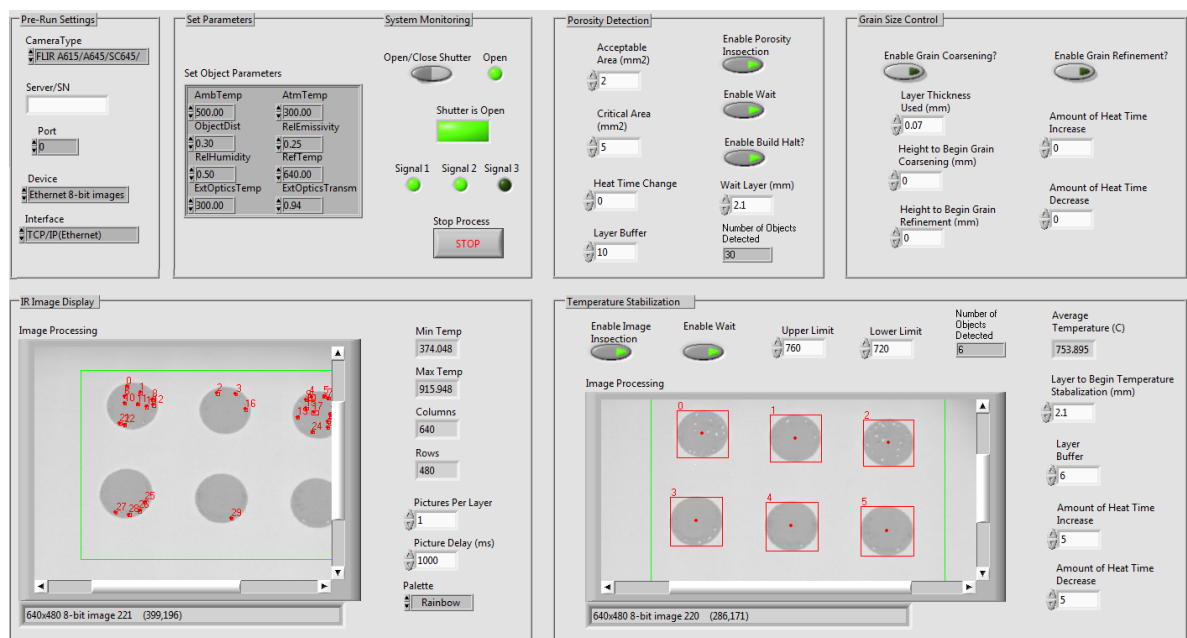


Figure 5 Functioning temperature stabilization interface showing part detection and temperature measurements

Intensity levels for previously identified porosity in IR images for EBM-fabricated parts has been measured and associated to object intensity levels in the virtual instrument's object detection algorithm to identify porosity during fabrication. Porosity in IR images can be seen in the fabricated parts shown in Figure 3 (b) for the standard and coarsened sections and are described by the red spots inside the melt area. Using the intensity threshold technique, porosity can be detected as shown in Figure 4. Based on the porosity measurements, a build can be stopped after potential porosity is detected or after a critical area of porosity is reached. Porosity detection is documented throughout the build and given to the operator for analysis of instances where porosity was detected that is useful for post-build analysis.

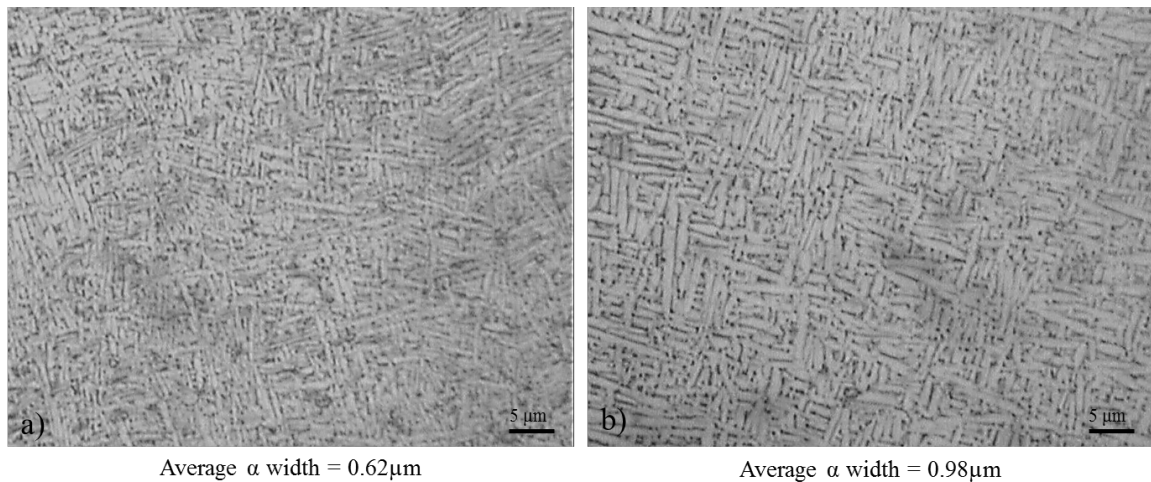


Figure 6 Microstructure of temperature stabilization algorithm for a) bottom section and b) top section

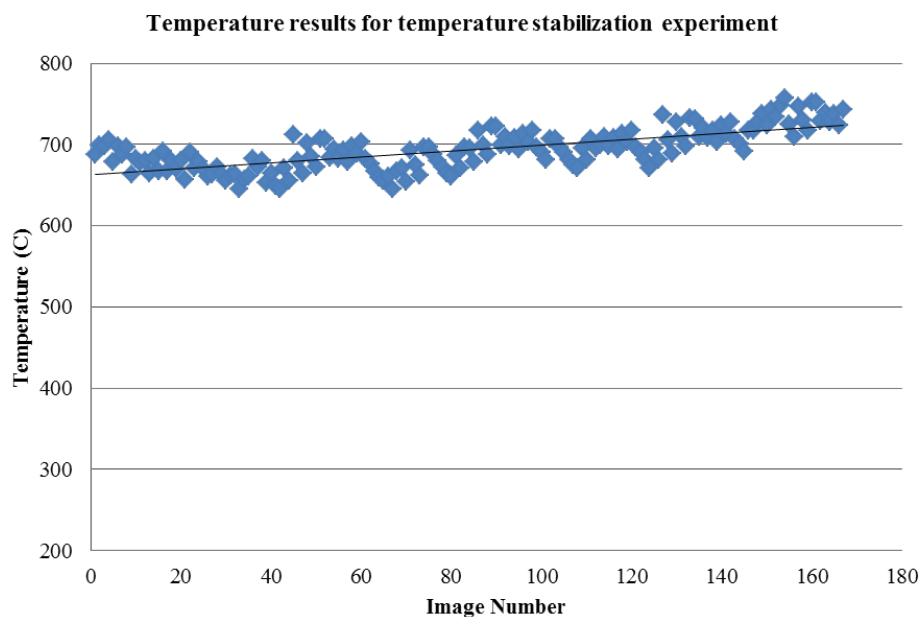


Figure 7 IR temperature results for temperature stabilization experiment

Conclusions

Using a previously installed IR camera in an Arcam A2 EBM system an improved image acquisition virtual instrument was created using LabVIEW software (Rodriguez, 2013). The improved virtual instrument allowed for automatic control of EBM technology to 1) achieve parameter modification using simulated mouse clicks useful for grain size control, 2) attempt temperature stabilization by recording a part's average temperature using image processing and automatically making decisions, 3) detect porosity during a build to determine if part fabrication needs to be stopped or porosity detection to be used for post-build analysis. Results show a grain size gradient was

achieved within a part but other part properties were also affected such as the development of porosity. Part detection and average temperature readings were taken to achieve temperature stabilization; however, development of part porosity presented a part quality problem when changing a single build parameter. Porosity in fabricated parts was successfully detected and can be used as a notification tool to a user in case an unacceptable level of porosity is reached and fabrication needs to stop. Porosity information can be used in the future to correct porosity via the control algorithm by parameter changes.

Future Work

Although a grain size gradient was achieved, it is still required to document parameter changes that produce a specific gain size. As previously mentioned, both time and temperature variables affect final grain size, therefore, variables affecting time that a part is left in the machine (e.g. height of build, heating/cooling time, overall size of part) may affect overall grain size and needs to be considered. For all automatic control operations, modification of parameters through simulated mouse clicks is not ideal since changes do not take effect immediately. Direct access to Arcam software would provide for instantaneous parameter changes instead of using mouse click simulations. Two computers were used in this study due to the high memory consumption of image processing that can affect computer processing causing build failure. Therefore a more powerful computer would be needed to mitigate possible communication issues or any communication delays that may occur.

References

- [1] Rodriguez, E., (2013). Development of a thermal imaging feedback control system in electron beam melting. Master's thesis for master's degree, University of Texas at El Paso, El Paso, Texas, USA.
- [2] Schwerdtfeger, J., Singer, R.F., Korner, C., (2012). In situ flaw detection by IR-imaging during electron beam melting. *Rapid Prototyping Journal*, 18 (4), pp. 259-263
- [3] Rodriguez, R., Medina, F., Espalin, D., Terrazas, C., Muse, D., MacDonald, E., Wicker, R., (2012). Integration of a thermal imaging feedback control system in electron beam melting. *Proceedings*
- [4] Puebla, K., Murr, L.E., Gaytan, S.M., Martinez, E., Medina, F., Wicker, R.B., (2012). Effect of melt scan rate on microstructure and macrostructure for electron beam melting of Ti-6Al-4V. *Materials Sciences and Applications*, 3, pp. 259-264.
- [5] Murr., L.E., Esquivel, E.V., Quinones, S.A., Gaytan, S.M., Lopez, M.I., Martinez, E.Y., Medina, F., Hernandez, D.H., Martinez, E., Martinez, J.L., Stafford, S.W., Brown, D.K., Hoppe, T., Meyers, W., Lindhe, U., Wicker, R.B., (2009). Microstructures and mechanical properties of electron beam-rapid manufactured

Ti-6Al-4V biomedical prototypes compared to wrought Ti-6Al-4V. Materials Characterization, 60, pp. 96-105

- [6] Porter, D.A., Easterling, K.E., (1981). Phase Transformations in Metals and Alloys. Chapman and Hall, London, pp. 139-143.
- [7] Al-Bermani, S.S., Blackmore, M.L., Zhang, W., Todd, I., (2010). The origin of microstructural diversity, texture, and mechanical properties in electron beam melted Ti-6Al-4V. The Minerals, Metals and Materials Society and ASM International, 41A, pp. 3422-3434.
- [8] Murr, L.E., Martinex, E., Gaytan, S.M., Ramirez, D.A., Machado, B.I., Shindo, P.W., Martinez, J.L., Medina, F., Wooten, J., Ciscel, D., Achelid, U., Wicker, R.B., (2011). Microstructural architecture, microstructures, and mechanical properties for a nickel-base superalloy fabricated by electron beam melting. Metallurgical and Materials Transactions, 42A, pp. 3491-3508.
- [9] Gil, F.J., Planell, J.A., (2000). Behaviour of normal grain growth kinetics in single phase titanium and titanium alloys. Materials Science and Engineering, A283, pp. 17-24.